

## ARTICLE OPEN



# Bioaerosols and dust are the dominant sources of organic P in atmospheric particles

Kalliopi Violaki<sup>1,2</sup>✉, Athanasios Nenes<sup>2,3</sup>, Maria Tsagkaraki<sup>4</sup>, Marco Paglione<sup>5</sup>, Stéphanie Jacquet<sup>1</sup>, Richard Sempéré<sup>1</sup> and Christos Panagiotopoulos<sup>1</sup>

Several studies assessed the impact of inorganic P in fertilizing oligotrophic areas, however, the importance of organic P in such fertilization processes received far less attention. In this study, the amount and origin of organic P delivered to the eastern Mediterranean Sea were characterized in atmospheric particles using the positive matrix factorization model (PMF). Phospholipids together with other chemical compounds (sugars, metals) were used as tracers in PMF. The model revealed that dominant sources of organic P are bioaerosols and dust. The amount of organic P from bioaerosols ( $\sim 4 \text{ Gg P y}^{-1}$ ) is similar to the amount of soluble inorganic P originating from dust aerosols; this is especially true during highly stratified periods when surface waters are strongly P-limited. The deposition of organic P from bioaerosols can constitute a considerable flux of bioavailable P—even during periods of dust episodes, implying that airborne biological particles can potentially fertilize marine ecosystems.

*npj Climate and Atmospheric Science* (2021)4:63; <https://doi.org/10.1038/s41612-021-00215-5>

## INTRODUCTION

Phosphorus (P) is critical to life on Earth, and its distribution in marine<sup>1</sup> and terrestrial ecosystems<sup>2</sup> is shaped by many biogeochemical processes. Inorganic P species (e.g., mono- or diprotated orthophosphate) comprise the most bioavailable P forms and have been studied for many decades. Organic phosphorous-containing compounds (org-P), such as nucleic acids, phospholipids, inositol phosphates, phosphoamides, phosphonates, phosphoproteins, sugar phosphates, and phosphonic acids, are thought to play a critical role in driving cell growth and metabolism, as well as the community composition of microorganisms<sup>3,4</sup>.

The org-P compounds are ubiquitous in organisms and thus contribute to the P biogeochemical cycle<sup>4</sup>. Although in the atmosphere primary biological particles (bioaerosols) are ubiquitous<sup>5</sup>, the amount and speciation of org-P are virtually unknown. Bioaerosols are composed of organic matter comprising cell fragments, pollen (diameter exceeding  $10 \mu\text{m}$ ), bacteria (diameter  $\sim 1 \mu\text{m}$ ), fungi, algae, moss, fern spores (diameter  $\sim 10 \mu\text{m}$ ), viruses (diameter less than  $0.1 \mu\text{m}$ ), and fragments from animals and plants<sup>6</sup>. Tracer-based emission rates of bioaerosol (as  $\text{PM}_{10}$  mass) for Europe is estimated at  $24 \text{ kg km}^{-2} \text{ y}^{-1}$ , with fungal spores and plant debris being the most important contributors to these emissions<sup>7</sup>. Dust also contains high concentrations of biological material, mainly from microorganisms or plant detritus<sup>8</sup>. This material may be enriched with additional biological loads (fungal spores, bacteria, viruses, pollen, etc.) through the adhesion of microbe-laden fine aquatic sprays to dust particles as the Sahara Desert plume moves over terrestrial and aquatic environments<sup>9</sup>.

Global modeling studies suggest that desert dust is a major source of P that contributes more than 82% to global P emissions ( $1.4 \text{ Tg P yr}^{-1}$ )<sup>10</sup>. The contribution of bioaerosols to P is 12% and could be as high as 45% in soluble P ( $0.5 \text{ Tg P yr}^{-1}$ , globally)<sup>11</sup>.

On the other hand, Wang et al. (2015)<sup>12</sup> indicated that combustion-related emissions of atmospheric P ( $1.8 \text{ Tg P yr}^{-1}$ ) represent over 50% of global atmospheric sources of P ( $3.5 \text{ Tg P yr}^{-1}$ ), suggesting that the perturbation of the global P cycle by anthropogenic emissions is greater than previously thought; however, these estimates are much higher than in other studies. These assessments highlight the uncertainties in understanding the role of atmospheric P in global biogeochemistry.

The Mediterranean Sea region has been identified as one of the most climate-sensitive marine ecosystems, with increased vulnerability owing to the effects of the increasing demographic and economic development occurring throughout its coastal zone. The long-term impacts on biogeochemical cycles and the ecosystem are highly uncertain<sup>13</sup>. Furthermore, the chronically P-limited Mediterranean Sea<sup>14</sup> is at a location, where anthropogenic pollution transported from continental Europe interacts with dust transported from the Sahara<sup>15,16</sup>, leading to a wide range of nutrient solubilization and deposition flux throughout the year. The eastern Mediterranean area is a low-nutrient, low-chlorophyll marine environment where bacterioplankton experience P limitation and phytoplankton experience co-limitation by nitrogen and phosphorus in the summer<sup>14,16</sup>. The seasonal Saharan dust storms enrich the atmosphere with plant debris, pollen, fungi and bacteria<sup>17</sup>. The polluted air masses from northern and central Europe, including summer biomass burning episodes are also influence the air quality of the area. These atmospheric inputs, with both natural and anthropogenic origin, represent an important source of new nutrients for marine ecosystems<sup>18–20</sup>.

The source apportionment analysis of P species, their quantitative impacts and the processes involved in the P biogeochemical cycle (especially for org-P) are poorly constrained in the study area. This paper estimates the source apportionment of atmospheric org-P by using a positive matrix factorization receptor model. The analysis was performed on the total suspended

<sup>1</sup>Aix Marseille Univ, Université de Toulon, CNRS, IRD, MIO, UM 110, 13288 Marseille, France. <sup>2</sup>Laboratory of Atmospheric Processes and their Impacts, School of Architecture, Civil & Environmental Engineering, École Polytechnique Fédérale de Lausanne, Lausanne 1015, Switzerland. <sup>3</sup>Center of Studies of Air Quality and Climate Change, Institute of Chemical Engineering Sciences, Foundation for Research and Technology Hellas, GR-26504 Patras, Greece. <sup>4</sup>Environmental Chemical Processes Laboratory (ECPL), Chemistry Department, University of Crete, 71003 Heraklion, Crete, Greece. <sup>5</sup>Italian National Research Council - Institute of Atmospheric Sciences and Climate (CNR-ISAC), Bologna, Italy. ✉email: kalliopi.violaki@epfl.ch

atmospheric particles (TSPs) collected from the eastern Mediterranean area over a one-year period to provide insights into the molecular diversity of key tracers, e.g., phospholipids that have never been reported for the area. Finally, the biogeochemical implications are discussed, and the P deposition attributed to different sources in the marine environment is estimated.

## RESULTS AND DISCUSSIONS

### Speciation of org-P

The analysis of the phospholipids (PLs) in the TSPs ( $n = 67$ ) revealed three main phospholipid classes: phosphatidylcholines (PCs), which were the most abundant PLs (73%), followed by phosphatidylglycerol (PG; 20%) and phosphatidylethanolamines (PEs; 7%). The average concentrations were  $10.9 \pm 25.9$  pmol P  $m^{-3}$  for the total PCs,  $3.0 \pm 2.9$  pmol P  $m^{-3}$  for PG and  $1.0 \pm 1.5$  pmol P  $m^{-3}$  for the total PEs. Among PCs,  $C_{44}H_{80}NO_8P$  was predominant (33%), followed by  $C_{42}H_{80}NO_8P$  (26%), while  $C_{39}H_{74}NO_8P$  was the most abundant PE (48%) (Supplementary Table 1). PCs ( $147.7$  pmol P  $m^{-3}$ ) and PEs ( $7.9$  pmol P  $m^{-3}$ ) exhibited the highest concentrations during the dust event recorded on the 5<sup>th</sup> of May 2017, at the same time as the highest concentration of org-P (Fig. 1, Supplementary Fig. 7).

The chemical structure of fatty acids esterified in PLs was determined by using MS/MS for each compound spectra. The most common fatty acids in PEs were oleic (C18:1, 27%), palmitic (C16:0, 26%), palmitoleic (C16:1, 24%), and linoleic acids (C18:2, 23%). The most dominant fatty acids identified in PCs were palmitic acid (C16:0, 27%) and palmitoleic acid (C16:1, 27%), followed by linoleic acid (C18:2, 14%), while stearic acid (C18:0, 2%) had a lower contribution. The presence of these fatty acids in the TSPs is in line with a previous study that identified palmitic, stearic, oleic, and linoleic acids as major constituents of cells in fungal and pollen species in outdoor air<sup>21</sup>. Many of these fatty

acids are unsaturated and consequently can be unstable in situ conditions, as they are rapidly oxidized and/or degraded in the atmosphere when they react with radicals (OH $\cdot$  and NO $_3\cdot$ ) and ozone<sup>22</sup>. The organic nitrates generated as oxidation products can serve as reservoirs for oxides of nitrogen that can be further decomposed to release NO $_x$  back to the atmosphere<sup>22</sup>.

### Sources of org-P compounds

Source apportionment was performed for the org-P compounds using the positive matrix factorization (PMF) approach (US EPA PMF 5.0 software). The model was applied to a combined dataset that included specific tracers, such as PLs and sugars, as well as other, more common tracers of aerosol sources, such as metals and ions. Specifically, levoglucosan and nss-K $^+$  were used as biomass burning tracers; nitrate, Pb, and V were used as tracers of anthropogenic sources; nss-SO $_4^{2-}$  and NH $_4^+$  were used as tracers of secondary processes; Al and nss-Ca $^{2+}$  were used as tracers of dust; mannitol and sucrose were used as tracers for fungi and pollen, respectively; PCs were used as tracers for eukaryotic cells; and Cl $^-$ , Mg $^{2+}$  and Na $^+$  were used as tracers of sea salts (Supplementary Table 8). Sources such as fertilizers or P in agricultural dust are not included here.

The PMF model apportioned seven principal sources: dust, biomass burning, sea salts, cells and pollen, fungi, anthropogenic sources and secondary sulfate (Fig. 1a). The principal source of org-P in terms of the relative contribution to each factor was bioaerosols (50.7%), represented here as the sum of cells/pollen (40.6%) and fungi (10.1%), followed by Saharan dust (23.9%) and anthropogenic sources (16.9%). The minor sources were secondary sulfate (4.6%) and marine sources (3.9%). These results confirm the importance of natural sources of org-P, especially bioaerosols and desert dust.

### The seasonal contribution of bioaerosols to org-P

Analysis of the month-to-month variability in org-P over the one-year sampling period revealed higher concentrations during spring, particularly in May ( $1.1 \pm 0.7$  nmol P  $m^{-3}$ ), than in winter (Fig. 1a). Sucrose also peaked in May at a concentration of  $392.9 \pm 271.5$  ng  $m^{-3}$ , which was seven times higher than the annual average. Sucrose is the dominant sugar component in airborne pollen grains, which play a significant role in regulating plant blossoming activity<sup>23</sup>. Pollen grains followed a clear seasonal cycle in the atmosphere in response to the plant flowering season<sup>24</sup>.

Maximum concentrations of both PCs and PEs were also observed in May, with average values of  $93.9 \pm 60.5$  pmol P  $m^{-3}$  and  $5.4 \pm 2.8$  pmol P  $m^{-3}$ , respectively. PLs are highly abundant in pollen grains, contributing  $\sim 38\%$  of the total lipids with contributions of 40 and 25% of the PC and PE classes, respectively<sup>25</sup>; the amount of PLs by weight is approximately 10-fold higher in pollen than in fungal spores<sup>21</sup>.

The results showed a significant correlation of sucrose with PCs ( $r = 0.90$ ,  $p < 0.0001$ , Supplementary Table 2), PEs ( $r = 0.84$ ,  $p < 0.001$ , Supplementary Table 2) and mannitol ( $r = 0.74$ ,  $p < 0.005$ ,  $r = 0.79$ ,  $p < 0.001$ , respectively, Supplementary Table 2) and the crustal elements (e.g., Al, Sr, Mn, nss-Ca $^{2+}$ , Supplementary Table 2), during the spring period. These results confirm that bioaerosols are an important vector of org-P that co-exist with dust, especially during the spring. Indeed, soil dust particles may contain organisms, including bacteria<sup>26</sup>, and they are considered excellent adsorptive surfaces for primary biological material, such as cell and fungal debris or pollen<sup>27</sup>. This primary biological material is the dominant source of PL compounds and can be transported far away from the sources<sup>27,28</sup>.

During summer, a correlation between org-P and PLs (neither with PCs and PEs nor PG; Supplementary Table 3) or other markers (e.g., mannitol or sucrose; Supplementary Table 3) was not found. Nevertheless, org-P exhibited a significant correlation with V,

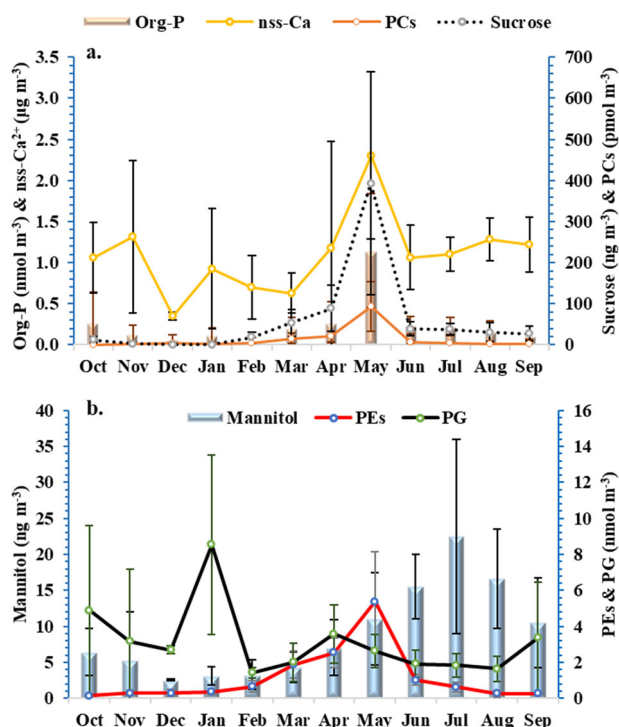


**Fig. 1** The monthly variation of org-P, along with bioaerosol tracers. **a** PCs, sucrose & dust tracer (nss-Ca $^{2+}$ ) and **(b)** mannitol, PEs, PG in total suspended particles over the eastern Mediterranean area. The error bars represent the standard deviation of the monthly average.

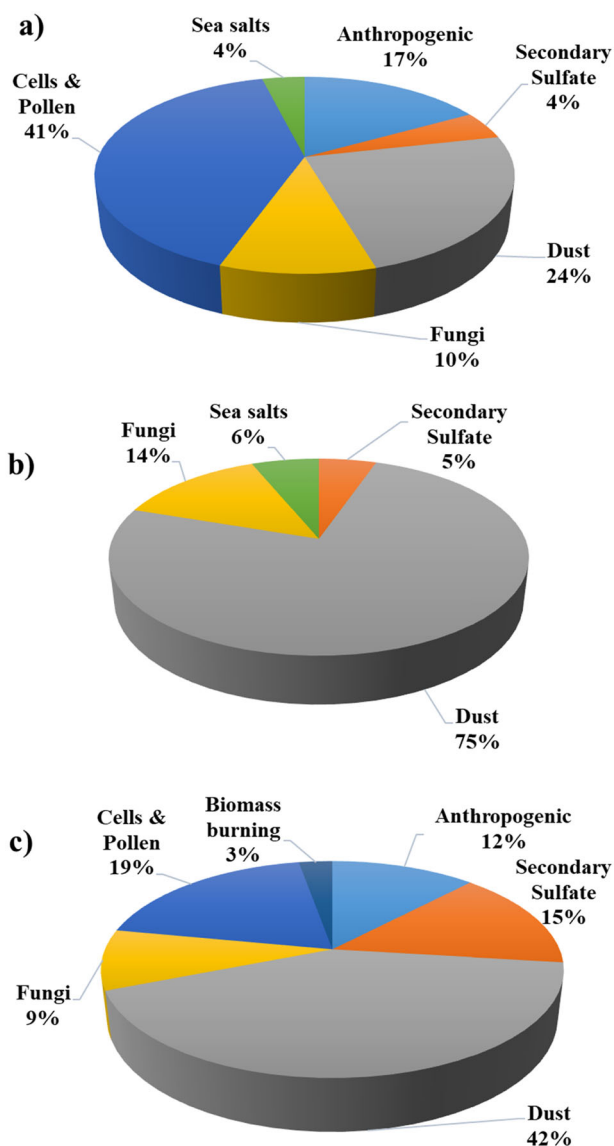


**Fig. 2** Percentage contribution of the sources to the P species. Source contribution of (a) org-P fraction, (b) Condensed P (CP), (c) Phosphate ions in atmospheric particles in the eastern Mediterranean area by using the approach of positive matrix factorization (PMF). CP are the condensed inorganic phosphates (pyro-, meta-, and other polyphosphates).

Zn and nitrate, which further suggests an anthropogenic origin considering that the air masses during summer originated mainly from central Europe. The detection of PLs during summer (Supplementary Table 6) indicated the presence of other types of cells, such as animal fragments, plant debris<sup>5</sup>, or marine bacteria. According to Mescioglu et al. (2019)<sup>29</sup>, 44% of common airborne bacteria, identified during non-dust conditions, were previously reported to be found in the Mediterranean Sea surface water.

Mannitol followed a different pattern than sucrose, with increased concentrations in summer and early autumn (Fig. 1b). These results indicate that mannitol inputs came from primary biogenic sources such as airborne fungal spores<sup>30</sup>, algae or various vascular plants<sup>31</sup>. This is significant for the eastern Mediterranean Sea because during that period, the stratification of surface waters is prevalent and external nutrient sources become more important. The correlation of PEs with mannitol in autumn

( $r = 0.62$ ,  $p < 0.05$ , Supplementary Table 4) further supports the common biological origin of these compounds from a biological source (e.g., fungi). However, org-P was significantly correlated only with PG in autumn ( $r = 0.54$ ,  $p < 0.05$ , Supplementary Table 4), while PG was significantly correlated with  $\text{Cl}^-$  ( $r = 0.58$ ,  $p < 0.05$ , Supplementary Table 4), suggesting the marine origin of PG and beyond the part of the org-P. Org-P was also correlated with crustal elements (e.g., Al, Sr, Mn, Supplementary Table 4), reflecting the impact of lithogenic sources.

In winter, org-P correlated significantly with PG ( $r = 0.86$ ,  $p < 0.0001$ , Supplementary Table 5),  $\text{Cl}^-$  ( $r = 0.75$ ,  $p < 0.05$ , Supplementary Table 5) and crustal elements (e.g., Al, Sr, Mn, Supplementary Tables 5 and 6), suggesting that the combination of marine cells with dust was the main contributor of org-P.

### The seasonality of org-P and the air mass origin influence the P speciation

The average annual concentration of total phosphorus (TP) in TSPs was  $0.67 \pm 0.56 \text{ nmol P m}^{-3}$  ( $n = 67$ ). Of the total concentration, 36% consisted of org-P, 40% of phosphate ions and 24% of CP (condensed P forms e.g., pyrophosphate or phosphorus minerals), with average concentrations of  $0.24 \pm 0.32$ ,  $0.25 \pm 0.22$  and  $0.18 \pm 0.23 \text{ nmol P m}^{-3}$ , respectively. High concentrations of TP and org-P species were observed during the dust event recorded on the 5<sup>th</sup> of May 2017 ( $2.72$  and  $1.66 \text{ nmol P m}^{-3}$ , respectively, Fig. 1a, Supplementary Fig. 7a), while the highest concentration of phosphate ions ( $1.21 \text{ nmol P m}^{-3}$ ) was measured during the dust event on the 8<sup>th</sup> of May 2017 (Supplementary Fig. 7b). A peak for CP was recorded during the dust event on 11<sup>th</sup> September 2017 ( $0.83 \text{ nmol P m}^{-3}$ , Supplementary Fig. 7c). The highest TP concentrations were associated with high mineral dust loadings during spring (Supplementary Table 6), which is consistent with previous studies<sup>10,32</sup>. The atmospheric concentration of all P species during the Saharan dust outbreaks was double what was recorded in air masses originating from central Europe and the Black Sea (Supplementary Table 7). The average TP values measured in this study in atmospheric particles originated from central Europe ( $0.5 \pm 0.3 \text{ nmol P m}^{-3}$ ,  $n = 21$ , Supplementary Table 7) and dust events in spring ( $2.0 \pm 1.0 \text{ nmol P m}^{-3}$ , Supplementary Table 6) are in line with those reported by Longo et al. (2014)<sup>33</sup> (TP of  $0.4 \pm 0.2$  and  $2.3 \pm 0.9 \text{ nmol P m}^{-3}$  for air masses originating from Europe and North Africa, respectively). The analysis of P-NEXFS in the latter study<sup>33</sup> revealed that org-P over the eastern Mediterranean area originated mainly from pollen and bacteria, which is in line with the data presented here.

The presence of bioaerosols and desert dust in the atmosphere significantly influenced the speciation of inorganic P over the eastern Mediterranean. The PMF results revealed that dust (74.9%) was the most important source of CP (Fig. 2b), followed by fungi (13.6%) and sea salts (6.2%). The loading of the inorganic P fraction was higher during dust events, mainly in autumn ( $0.38 \pm 0.31 \text{ nmol P m}^{-3}$ , Supplementary Table 6). High concentrations were also present ( $0.42 \pm 0.24 \text{ nmol P m}^{-3}$ , Supplementary Table 6) in summer, when air masses from the Black Sea prevailed, suggesting soil transport from arid regions of eastern Europe.

The source apportionment analysis carried out with PMF (Fig. 2c) showed that the principal source for phosphate ions was dust (42.1%), followed by bioaerosols (28.2%), secondary sulfate (14.8%), anthropogenic sources (12.1%) and biomass burning (2.8%). The highest phosphate ion concentrations were observed in spring during dust events ( $0.82 \pm 0.39 \text{ nmol P m}^{-3}$ , Supplementary Table 6). The phosphate ions were also detected in pollen grains, contributing 60% of the total phosphorus in pollen<sup>34</sup>. The percentage anthropogenic contribution in phosphate sources in this study was similar to the global percentage of 14.3% proposed by Mahowald et al. (2008)<sup>10</sup>.



**Table 1.** Estimated annual deposition fluxes of organic carbon, organic nitrogen and phosphorus originating from PLs compounds quantified in this study in East Mediterranean atmosphere.

Annual	$\mu\text{mol C m}^{-2}$	$\mu\text{mol N m}^{-2}$	$\mu\text{mol P m}^{-2}$
PCs	350.6	8.3	8.3
PEs	28.7	0.7	0.7
PG	50.9	–	2.0
<b>Total</b>	<b>430.2</b>	<b>9.0</b>	<b>11.0</b>

### Estimation of PLs fluxes from the atmosphere into the eastern Mediterranean sea

PLs are among the major reservoirs of phosphorus in marine plankton<sup>35</sup>. The depletion of PLs observed in open ocean surface seawater implies that they are rapidly assimilated once they are released to the marine environment, as they serve as a P source for heterotrophic bacteria<sup>36</sup>. Our results suggest that the atmosphere is a potential source of PLs for the marine environment; therefore, their atmospheric flux was calculated. The flux,  $F$ , of PLs (via dry deposition) was estimated using the equation  $F = -V_d C$ , where  $F$  is the flux in  $\text{mol m}^{-2} \text{d}^{-1}$ ,  $C$  is the concentration of atmospheric particles in  $\text{mol m}^{-3}$  and  $V_d$  is the deposition velocity in  $\text{m s}^{-1}$ . Studies of nutrients and trace metals in the eastern Mediterranean performed with size-segregated aerosol sampling<sup>37</sup> revealed that a coarse particle deposition velocity of  $2 \text{ cm s}^{-1}$  could be applied for flux estimation in the area. Assuming that PLs are mainly in coarse particles, as they are strongly correlated with pollen grains, the estimated annual deposition of PLs was  $11.0 \mu\text{mol P m}^{-2} \text{y}^{-1}$  (Table 1). When this flux is scaled to the eastern Mediterranean surface<sup>37</sup> ( $1.67 \times 10^{12} \text{ m}^2$ ), the total annual deposition of P to the basin was estimated at  $0.6 \text{ Gg P}$  of org-P.

Similarly, to the estimated P deposition, the estimated annual deposition of carbon attributed to phospholipids was calculated theoretically at  $430.2 \mu\text{mol C m}^{-2} \text{y}^{-1}$  (Table 1). This is comparable with the annual total deposition of primary sugars (i.e., fructose, glucose, sucrose:  $629.2 \mu\text{mol C m}^{-2} \text{y}^{-1}$ ) precipitated in the area<sup>38</sup>. Extrapolating this carbon flux to the eastern Mediterranean surface, the annual C deposited to the basin was estimated at  $8.6 \text{ Gg}$  of carbon. The contribution of phospholipids in terms of organic nitrogen was minimal (only PCs and the PEs have N in their structure). The theoretical dry deposition of organic N was calculated at  $9.0 \mu\text{mol N m}^{-2}$  (Table 1), representing only 0.2% of the organic nitrogen deposited in the area<sup>39</sup>.

The results of this study indicated that PLs account for  $\sim 8\%$  of org-P on average, suggesting that most of this pool remains chemically uncharacterized, with unknown bioavailability. However, considering that more than half of the org-P compounds originated from bioaerosols, this fraction could at least be potentially bioavailable. This is because the most common functional groups in those biological org-P compounds are the monophosphate esters (e.g., phosphoserine, sugar phosphates) or diphosphate esters found in nucleotides and their derivatives (e.g., DNA, RNA, AMP, ADP, ATP), as well as PLs<sup>40</sup>. The majority of the above compounds have a C-O-P bond that is easily hydrolysable in the marine environment by the alkaline phosphatase enzyme<sup>39</sup>, unlike the slow hydrolysis of C-P compounds such as phosphonates<sup>41,42</sup>. This is in agreement with Djaoudi et al. (2018)<sup>43</sup>, who estimated that on average,  $44 \pm 27\%$  of the atmospheric org-P deposited in the Mediterranean is bioavailable.

### Deposition fluxes of P species attributed to their sources

Based on the results of the source apportionment analysis carried out by PMF (Fig. 2) and the atmospheric concentrations of

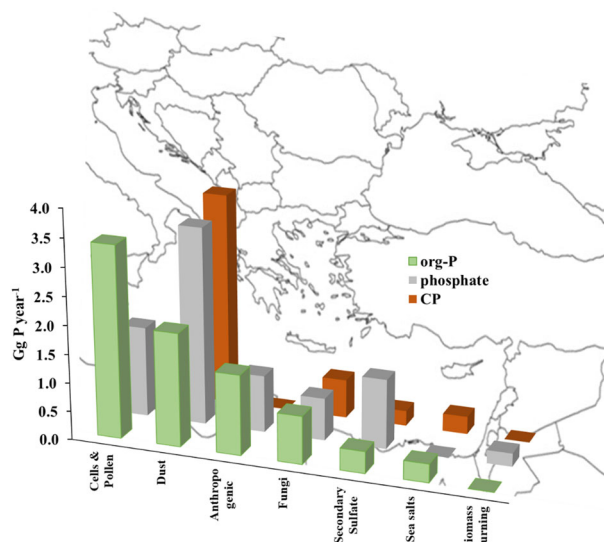


**Fig. 3 Annual deposition fluxes of P species.** Estimation of the annual deposition fluxes (in  $\text{Gg P year}^{-1}$ ) of phosphorus species and their distribution to different sources over the eastern Mediterranean during one-year period (2016–2017) for total suspended particles. Total P was calculated to be  $21.5 \text{ Gg P year}^{-1}$ .

P species, the maximum annual deposition scaled to the eastern Mediterranean surface was calculated (Fig. 3). Annually, a total of  $21.5 \text{ Gg P}$  was deposited in the basin, with an almost equal deposition of org-P and phosphate ions (Fig. 3). Dust was a major source of inorganic P forms and was responsible for almost equal contributions of phosphate ions and condensed P forms (e.g., pyrophosphate or phosphorus minerals). Bioaerosols were a source of a similar magnitude for org-P compounds, with an annual deposition of  $4.2 \text{ Gg P}$  in the eastern Mediterranean (Fig. 3). Anthropogenic pollution contributed slightly more to org-P than phosphate ions, and the latter were produced mainly secondarily. Biomass burning emissions in the area were associated mainly with more soluble P<sup>44</sup>.

It is worth noting that the contribution of biogenic P to the global TP is suggested by global transport models to be 12%, and the contribution of dust is estimated to be 82%<sup>9,10</sup>. In the case of the eastern Mediterranean area, the contribution of bioaerosols (including both fungi and pollen) was higher, at 33% of the deposited TP, while the contribution of dust was 43% (Supplementary Fig. 8).

Considering a P solubility value of 73% for the eastern Mediterranean<sup>45</sup>, the dissolved P was estimated to be  $15.7 \text{ Gg P}$ . To calculate the maximum impact of total dissolved phosphorus deposition in marine ecosystems, we assumed that all dissolved P was bioavailable. Converting the P flux into carbon uptake using the Redfield C:P ratio of 106, the dissolved P was found to be responsible for the fixation of  $0.6 \text{ Tg C y}^{-1}$ , which is within the range proposed by Kanakidou et al. (2020)<sup>46</sup>. Assuming an annual new production for the eastern Mediterranean<sup>47</sup> on the order of  $7 \text{ Tg C y}^{-1}$  according to the above calculation, the atmospheric deposition of dissolved P may contribute as much as 9% to the new primary production in the eastern Mediterranean. With recent observations and modeling studies predicting a decrease in primary productivity due to warming climate<sup>48</sup>, causing an enhancement in stratification, atmospheric deposition of dissolved P could play a more important role in the future especially for a low production area like the eastern Mediterranean Sea.

## METHODS

### Sampling site

Sampling was conducted on the island of Crete, Greece, for a one-year period starting in October 2016 (Supplementary Fig. 1). A high-volume TSPs sampler (TISCH) was used to collect atmospheric particles on precombusted (450 °C for 6 h) 20 × 25 cm quartz filters (Pall, 2500QAT-UP). The sampling resolution was 48 h, at a flow rate of 85 m<sup>3</sup> h<sup>-1</sup>. Sampling was carried out on the north side of the Department of Chemistry building, University of Crete (35° 18'N, 25°45'E), located at a semirural site approximately 6 km from the city of Heraklion.

### Chemicals and reagents

Ultrapure water (Milli-Q system, 18 MΩ.cm) was used to prepare all aqueous solutions. Acetonitrile and ammonium acetate were purchased from Sigma Aldrich (LC-MS grade). 1,2-Dimyristoyl-sn-glycero-3-phosphocholine (Sigma Aldrich: P2663) and 1,2-dimyristoyl-sn-glycero-3-phosphoethanolamine (Sigma Aldrich: P5693) were used as standards for the quantification of phosphatidylcholines (PCs) and phosphatidylethanolamines (PEs), respectively. Phosphatidylglycerol (PG) was quantified using the standard (10:0):1,2-didecanoyl-sn-glycero-3-phospho-(1'-rac-glycerol) (sodium salt) (840434, Avanti Polar Lipids Inc).

### Analysis of PLs

Part of each quartz filter (~40 cm<sup>2</sup>) was extracted with 5 ml of MeOH by sonication for 20 min. Then, the suspended particles were removed by centrifugation at 5000 g for 5 min. The supernatant was transferred to glass pipets in injection vials for analysis. All glassware was combusted at 450 °C for 5 h to eliminate organics. Chemical analyses were performed by an Agilent LC-ESI-Q-TOF/MS system equipped with an LC system (Agilent 1290 Infinity) coupled with a Q-TOF (Agilent 6530 Accurate-Mass). Chromatographic separation (Supplementary Fig. 2) was performed with a Luna-HILIC (Phenomenex) column (100 mm, 2 mm I.D., 3 μm particle size). Gradient chromatographic separation was achieved by using H<sub>2</sub>O as the mobile phase with 5 mM ammonium acetate (A) and acetonitrile with 5 mM ammonium acetate (B). The gradient elution was 1) 10% (A) from 0–2.5 min, 2) 50% (A) from 2.5–10 min, 3) 50% (A) from 10–12 min, 4) 10% (A) from 12–14 min, and 5) 10% (A) from 14–17 min. The flow rate was set at 100 μl min<sup>-1</sup>. The column temperature was set at 25 °C, and the injection volume was 2 μl. Ionization was performed in positive mode using the following operational parameters: capillary voltage, 3500 V; drying gas, 8 L min<sup>-1</sup>; nebulizer pressure, 35 psig; gas temperature, 350 °C; sheath gas temperature, 300 °C; sheath gas flow, 11 L min<sup>-1</sup>; nozzle voltage, 1000 V; fragmentor voltage, 160 V; skimmer voltage, 65 V; and octopole RF, 750 V. The full scan MS data were recorded at a rate of 1 spectra s<sup>-1</sup> in the range of m/z 50–1700 at 2 GHz. All the MS data were recorded with Agilent Mass Hunter Data Acquisition (B.05.00) and processed by Agilent Mass Hunter Qualitative Analysis (B.05.00). MS/MS experiments were carried out with a medium isolation width (~4 amu) and a fixed collision energy of 50 eV for all the compounds. The instrument was calibrated daily before starting the analysis using the calibration solution provided by the manufacturer.

### PLs quantification

The chemical characterization of PLs was performed based on the identification of specific ions, recorded as [M + H]<sup>+</sup>, [M + Na]<sup>+</sup> and [M + K]<sup>+</sup> adducts for PCs; [M + H]<sup>+</sup>, [M + Na]<sup>+</sup> for PEs; and [M + Na]<sup>+</sup> for PG (Supplementary Table 1; Supplementary Fig. 3). PCs were identified from the MS/MS spectra as the protonated ion [M + H]<sup>+</sup> at m/z 184.0733. PEs were identified by the neutral loss of fragments at m/z 141.0191. PG was identified by the loss of fragments at m/z 189.5026 as phosphoglycerol with an NH<sub>4</sub><sup>+</sup> adduct. For the quantification of phosphatidylcholines (PCs), the protonated ion [M + H]<sup>+</sup> at m/z 184.0733 from MS/MS spectra was integrated. Phosphatidylethanolamines (PEs) were quantified from full scan mode spectra with the extracted ion fragments referred to in supplementary Table 1. PG was quantified from full scan mode spectra with the extracted ion fragment at m/z 577.5026 by using the PG standard (10:0). The matrix effect was eliminated significantly by diluting the samples 10 times with MeOH prior to injection. The detection limits were 0.3, 3.0, and 4.0 pg for PC, PE, and PG, respectively, for a 2 μl injection volume.

### Analysis of main ions

Part of each quartz filter (~1.5 cm<sup>2</sup>) was extracted with 4 ml of ultrapure water (Milli-Q system, 18 MΩ.cm) by sonication for 45 min. The extraction efficiency of this method was higher than 98% for all the above ions. Extracted samples were stored in the dark until analysis after the addition of chloroform (100–150 μl). The main anions (Cl<sup>-</sup>, NO<sub>3</sub><sup>-</sup>, SO<sub>4</sub><sup>2-</sup>, HPO<sub>4</sub><sup>2-</sup>, C<sub>2</sub>O<sub>4</sub><sup>2-</sup>) in the aerosol extractions were analyzed by ion chromatography (IC) after separation on a Dionex AS4A-SC column. All the anions were determined with isocratic elution at 1.5 mL min<sup>-1</sup> with Na<sub>2</sub>CO<sub>3</sub>/NaHCO<sub>3</sub> eluent, and an ASRS-300 4 mm suppressor in autosuppression mode was used. For the cations (Na<sup>+</sup>, NH<sub>4</sub><sup>+</sup>, K<sup>+</sup>, Mg<sup>2+</sup>, and Ca<sup>2+</sup>), a CS12-SC column with a CSRS-300 4 mm suppressor was used. Separation was achieved under isocratic conditions with methanesulfonic acid (MSA) eluent (20 mM) and a flow rate of 1.0 mL min<sup>-1</sup>. The detection limit ranged from 1 to 5 ppb for the main anions and cations and was 3 ppb for phosphate ions. The blanks were always below the detection limits.

### Trace metals and total phosphorus analysis

Part of each quartz filter (~8 cm<sup>2</sup>) was digested with 5 ml of HNO<sub>3</sub> by using a microwave digester and analyzed for Al, Ca, Mn, Fe, trace metals (V, Cr, Ni, Cu, Zn, Cd, and Pb), and total phosphorus (TP) with a high resolution inductively coupled plasma mass spectrometer (HR-ICP-MS; ELEMENT XR, Thermo). A microwave digestion system (Anton Paar Multiwave 3000) with Teflon vessels and concentrated distilled nitric acid (puriss. p.a., Fluka Prod. No. 84380) was used. The heating program applied was two steps of 30 min heating at 180 °C and 999 W of microwave power followed by a third step of 20 min heating at 100 °C and 800 W of microwave power. After cooling to room temperature, the digested solution was transferred to acid-cleaned polyethylene tubes and stored in the freezer prior to HR-ICP-MS analysis. The instrument was calibrated externally using standard solutions, and indium was used as an internal standard. Quality control of the digestion procedure and of the HR-ICP-MS measurements was performed by determining the element concentrations of certified reference materials (MESS-4, SLRS-5, SLEW3 and CASS-5). The recoveries obtained for certified reference materials ranged from 90 to 104% for all studied elements except Al (60%), which was corrected accordingly. The detection limit, defined as three times the standard deviation of the blank value, was below 3 ppt.

### Phosphorus speciation

The speciation of P in atmospheric particles was determined according to the analytical protocol described by Violaki et al. (2018)<sup>45</sup>. TP was measured after the acid digestion of samples by HR-ICP-MS, and the TP recoveries obtained with the use of certified reference materials (MESS-4) ranged from 98 ± 12%. The dissolved inorganic phosphorus was determined to be phosphate ions by IC, while the total acid hydrolyzed inorganic phosphorus (TIP) was determined after mild oxidation of the filter sample (pH = 1.6) with sulfuric acid (0.02 M). The total organic-bound phosphates (org-P) were determined by subtracting TIP from TP. The condensed phosphates (pyro-, meta-, and other polyphosphates), called CP, were determined by subtracting phosphate ions from TIP.

### Sugars analysis

Part of each quartz filter (~40 cm<sup>2</sup>) was extracted with 5 ml of ultrapure water (Milli-Q system, 18 MΩ.cm) by sonication for 45 min. The chemical analysis of sucrose, mannitol and anhydrosugars (the sum of levoglucosan, manosan and galactosan) was performed with the same LC-ESI-Q-TOF/MS system. Chromatographic separation was performed with a Luna-HILIC (Phenomenex) column (100 mm, 2 mm I.D., 3 μm particle size). Gradient chromatographic separation was achieved by using H<sub>2</sub>O with 5 mM ammonium acetate (A) as the mobile phase and acetonitrile with 5 mM ammonium acetate (B). The gradient elution program was 1) 40% (A) from 0–3.5 min, 2) 50% (A) from 3.5–8 min, 3) 90% (A) from 8–10 min, and 4) 40% (A) from 10–12 min. The flow rate was set at 100 μl min<sup>-1</sup>. The column temperature was set at 25 °C, and a 5 μl volume injection was used. Ionization was performed in positive mode using the following operational parameters: capillary voltage, 3500 V; drying gas, 12 L min<sup>-1</sup>; nebulizer pressure, 40 psig; gas temperature, 250 °C; sheath gas temperature, 250 °C; sheath gas flow, 11 L min<sup>-1</sup>; nozzle voltage, 1000 V; fragmentor voltage, 100 V; skimmer voltage, 65 V; and octopole RF, 750 V. The full scan MS data were recorded at a rate of 1 spectrum min<sup>-1</sup> in the range of m/z 100–1700 at 2 GHz. All the MS data were recorded with Agilent Mass Hunter Data

Acquisition (B.05.00) and processed by Agilent Mass Hunter Qualitative Analysis (B.05.00). The sugars were detected as  $[M + Na]^+$  adducts at typical fragments of  $m/z$  365.1054,  $m/z$  185.0420, and  $m/z$  205.0693 for sucrose, levoglucosan and mannitol, respectively, with detection limits at 17, 22, and 24 pg, respectively, for a 5  $\mu$ l injection volume.

### Positive matrix factorization (PMF)

The goal of receptor models such as PMF is to solve the chemical mass balance (CMB) equation between the measured species concentrations and the source profiles, as shown in the following equation:

$$X = G \times F + E$$

In the field of atmospheric science, if the X matrix is the concentration of species at a given receptor site, the G matrix is the contribution of a "source" factor, the F matrix is the chemical profile of this factor, and E is the matrix of the residuals, i.e., the unexplained part of X.

The U.S. Environmental Protection Agency (US-EPA) PMF5.0 software<sup>49</sup> was used in the present study to perform source apportionment for the P compounds, following the general recommendation guidelines of the European Joint Research Centre<sup>50</sup>. A range of solutions with different numbers of factors (2–10) was examined here, and 7 factors were the maximum number of factors corresponding to meaningful sources (Supplementary Fig. 4, Supplementary Fig. 5, Supplementary Fig. 6). The characteristic tracers for the identification of the PMF factors are presented in Supplementary Table 8. If the factors were increased, some profiles were split, creating profiles with no physical meaning. The selection of input variables was based on the availability of the species in the highest number of samples ( $n = 67$ ) and the value of the signal-to-noise ratio (S/N) for each species. Values lower than the detection limit (d. L.) were set to d. L./2, with uncertainties equal to  $5/6 \times d. L.$ , following Polissar et al. (1998)<sup>50</sup>. The extra modeling uncertainty was adjusted to 10%. The uncertainties were calculated according to the equation  $Unc = \sqrt{[(\text{error fraction} \times \text{concentration})^2 + (0.5 \times d.L.)^2]}$ . In the current study, the variables mass, CP, org-P, PG, nss-K, Pb, and V were set as "weak"<sup>51</sup>. There were no "bad" values. The statistical representativeness of the solution was evaluated using a bootstrap test (BS), Displacement (DISP), and BS-DISP (Bootstrap + Displacement) for 100 successive iterations of the model and for a minimum correlation  $r^2$  of 0.6 (Supplementary Table 9). Additionally, the evolution of the ratio  $Q_{true}/Q_{robust}$  ( $< 1.5$ ) was performed; here, the solution has a  $Q_{true}/Q_{robust}$  ratio of 1, indicating zero impact of outliers on the results. The unexplained mass from PMF model was 3%. The weighted residuals for most of the species had a normal centered distribution, indicating an overall good modeling of most variables.

### DATA AVAILABILITY

The data that support the findings of this study are available from the corresponding author upon request.

Received: 26 February 2021; Accepted: 27 October 2021;

Published online: 03 December 2021

### REFERENCES

- Hansell D. A. & Carlson G. A. *Biogeochemistry of Marine Dissolved Organic Matter*. 2nd edn, (Elsevier, 2015).
- Hou, E. et al. Global meta-analysis shows pervasive phosphorus limitation of aboveground plant production in natural terrestrial ecosystems. *Nat. Commun.* **11**, 637 (2020).
- Dyrman, S. T., Ammerman, J. W. & Van Mooy, B. A. S. Microbes and the marine phosphorus cycle. *Oceanography* **20**, 110–116 (2007).
- Turner, B. L., Frossard, E., Baldwin, D. S. *Organic Phosphorus in the Environment*. 1st edn, (CABI Publishing, 2005).
- Fröhlich-Nowoisky et al. Bioaerosols in the Earth system: climate, health, and ecosystem interactions. *Atmos. Res.* **182**, 346–376 (2016).
- Després et al. Primary biological aerosol particles in the atmosphere: a review. *Tellus B* **64**, 015598 (2012).
- Winiwarter, W., Bauer, H., Caseiro, A. & Puxbaum, H. Quantifying emissions of primary biological aerosol particle mass in Europe. *Atmos. Environ.* **43**, 1403–1409 (2009).
- Griffin, D. W. & Kellogg, C. A. Dust Storms and Their Impact on Ocean and Human Health: dust in Earth's Atmosphere. *Eco Health* **1**, 284–295 (2004).
- Griffin, D. W. Atmospheric movement of microorganisms in clouds of desert dust and implications for human health. *Clin. Microbiol. Rev.* **20**, 459–477 (2007).
- Mahowald, N. et al. Global distribution of atmospheric phosphorus sources, concentrations and deposition rates, and anthropogenic impacts. *Glob. Biogeochem. Cycles* **22**, GB4026 (2008).
- Myriokefalitakis, S., Nenes, A., Baker, A. R., Mihalopoulos, N. & Kanakidou, M. Bioavailable atmospheric phosphorus supply to the global ocean: a 3-D global modeling study. *Biogeosciences* **13**, 6519–6543 (2016).
- Wang, R. et al. Significant contribution of combustion-related emissions to the atmospheric phosphorus budget. *Nat. Geosci.* **8**, 48–54 (2015).
- The Mermex Group. Marine ecosystems responses to climatic and anthropogenic forcing in the Mediterranean. *Prog. Oceanogr.* **91**, 97–166 (2011).
- Krom, M. D. et al. Nutrient cycling in the south east Levantine basin of the eastern Mediterranean: results from a phosphorus starved system. *Deep Sea Res. Part II* **52**, 2879–2896 (2005).
- Guerzoni, S. et al. The role of atmospheric deposition in the biogeochemistry of the Mediterranean Sea. *Prog. Oceanogr.* **44**, 147–190 (1999).
- Pitta, P. et al. Biological response to P addition in the Eastern Mediterranean Sea. The microbial race against time. *Deep Sea Res. Part II* **52**, 2961–2974 (2005).
- Griffin Dale, W. et al. Airborne desert dust and aeromicrobiology over the Turkish Mediterranean coastline. *Atmos. Environ.* **41**, 4050–4062 (2007).
- Markaki, Z., Loye-Pilot, M. D., Violaki, K., Benyahya, L. & Mihalopoulos, N. Variability of atmospheric deposition of dissolved nitrogen and phosphorus in the Mediterranean and possible link to the anomalous seawater N/P ratio. *Mar. Chem.* **120**, 187–194 (2010).
- Herut, B. et al. The Potential Impact of Saharan Dust and Polluted Aerosols on Microbial Populations in the East Mediterranean Sea, an Overview of a Mesocosm Experimental Approach. *Front. Mar. Sci.* **3**, 226 (2016).
- Pitta, P. et al. Saharan Dust Deposition Effects on the Microbial Food Web in the Eastern Mediterranean: A Study Based on a Mesocosm Experiment. *Front. Mar. Sci.* **4**, 117 (2017).
- Womilaju, T. O., Miller, J. D., Mayer, P. M. & Brook, J. R. Methods to determine the biological composition of particulate matter collected from outdoor air. *Atmos. Environ.* **37**, 4335–4344 (2003).
- Estillore, A., Trueblood, J. V. & Grassian, V. H. Atmospheric chemistry of bioaerosols: heterogeneous and multiphase reactions with atmospheric oxidants and other trace gases. *Chem. Sci.* **7**, 6604–6616 (2016).
- Fu, P., Kimitaka, K., Kobayashi, M., Bernd, R. T. & Simoneit Seasonal variations of sugars in atmospheric particulate matter from Gosan, Jeju Island: Significant contributions of airborne pollen and Asian dust in spring. *Atmos. Environ.* **55**, 234–239 (2012).
- Tormo-Molina Rafael, M. A., Gonzalo-Garrijol Silva-Palacios, A. & Muñoz-Rodríguez, F. General Trends in Airborne Pollen Production and Pollination Periods at a Mediterranean Site (Badajoz, Southwest Spain) *J. Investig. Allergol. Clin. Immunol.* **20**, 567–574 (2010).
- Andrikopoulos, K. N., Sifaka-Kapadai, A., Demopoulos, A. C. & Kapoulas, M. V. Lipids of pinus halepensis pollen. *Phytochem* **24**, 2953–2957 (1985).
- Belov, A. A., Cheptsov, V. S. & Vorobyova, E. A. Soil bacterial communities of Sahara and Gibson deserts: Physiological and taxonomical characteristics. *Aim. Microbiol.* **4**, 685–710 (2018).
- Prospero, J., Blades, E., Mathison, G. & Naidu, R. Interhemispheric transport of viable fungi and bacteria from Africa to the Caribbean with soil dust. *Aerobiologia* **21**, 1–19 (2005).
- Kellogg, C. A. & Griffin, D. W. Aerobiology and the global transport of desert dust. *Trends Ecol. Evol.* **21**, No.11 (2009).
- Mescioglou, E. et al. Aerosol Microbiome over the Mediterranean Sea Diversity and Abundance. *Atmosphere* **10**, 440 (2019).
- Bauer, H. et al. Arabitol and mannitol as tracers for the quantification of airborne fungal spores. *Atmos. Environ.* **42**, 588–593 (2008).
- Iwamoto, K. & Shiraiwa, Y. Salt-Regulated Mannitol Metabolism in Algae. *Mar. Biotechnol.* **7**, 407–415 (2005).
- Vet, R. et al. A global assessment of precipitation chemistry and deposition of sulfur, nitrogen, sea salt, base cations, organic acids, acidity and pH, and phosphorus. *Atmos. Environ.* **93**, 3–100 (2014).
- Longo, F. A. et al. P-NEXFS analysis of aerosol phosphorus delivered to the Mediterranean Sea. *Geophys. Res. Lett.* **41**, 4043–4049 (2014).
- Doskey, P. V. & Ugoagwu, B. J. Atmospheric deposition of macronutrients by pollen at a semi-remote site in northern Wisconsin. *Atmos. Environ.* **3**, 2761–2766 (1989).
- Van Mooy, B. A. S., Rocap, G., Fredricks, H. F., Evans, C. T. & Devol, A. H. Sulfolipids dramatically decrease phosphorus demand by picocyanobacteria in oligotrophic marine environments. *Proc. Natl Acad. Sci. USA* **103**, 8607–8612 (2006).
- Suzumura, M. Phospholipids in marine environments: a review. *Talanta* **66**, 422–434 (2005).
- Theodosi, C. et al. Sugars in atmospheric aerosols over the Eastern Mediterranean. *Prog. Oceanogr.* **163**, 70–81 (2018).



38. Candela, J. & Winant, C. D. Meteorologically forced sub inertial flows through the strait of Gibraltar. *J. Geophys. Res.* **94**, 12667–12679 (1989).
39. Violaki, K., Zarbas, P. & Mihalopoulos, N. Long-term measurements of dissolved organic nitrogen (DON) in atmospheric deposition in the Eastern Mediterranean: Fluxes, origin and biogeochemical implications. *Mar. Chem.* **120**, 179–186 (2010).
40. Van Wambeke, F. et al. Dynamics and controls of heterotrophic prokaryotic production in the western tropical South Pacific Ocean: links with diazotrophic and photosynthetic activity. *Biogeosciences* **15**, 2669–2689 (2018).
41. White, A. E., Watkins-Brandt, K. S., Engle, M. A., Burkhardt, B. & Paytan, A. Characterization of the rate and temperature sensitivities of bacterial remineralization of dissolved organic phosphorus compounds by natural populations. *Front. Microbiol.* **3**, 1–13 (2012).
42. Sosa, A. O. et al. Isolation and characterization of bacteria that degrade phosphonates in marine dissolved organic matter. *Front. Microbiol.* **8**, 1786 (2017).
43. Djaoudi, K. et al. Atmospheric fluxes of soluble organic C, N, and P to the Mediterranean Sea: Potential biogeochemical implications in the surface layer. *Prog. Oceanogr.* **163**, 59–69 (2018).
44. Barkley, E. A. et al. African biomass burning is a substantial source of phosphorus deposition to the Amazon, Tropical Atlantic Ocean, and Southern Ocean. *PNAS* **116**, 16216–16221 (2019).
45. Violaki, K. et al. Organic phosphorus in atmospheric deposition over the Mediterranean Sea: An important missing piece of the phosphorus cycle. *Prog. Oceanogr.* **163**, 50–58 (2018).
46. Kanakidou, M., Myriokefalitakis, S. & Tsagkaraki, M. Atmospheric inputs of nutrients to the Mediterranean Sea. *Deep Sea Res. Part II: Topical Stud. Oceanogr.* **171**, 104606 (2020).
47. Kress, N. & Herut, B. Spatial and seasonal evolution of dissolved oxygen and nutrients in the Southern Levantine Basin (Eastern Mediterranean Sea): chemical characterization of the water masses and inferences on the N:P ratios. *Deep-Sea Res. Part I* **48**, 2347–2372 (2001).
48. Adloff, F. et al. Mediterranean Sea response to climate change in an ensemble of twenty first century scenarios. *Clim. Dyn.* **45**, 2775–2802 (2015).
49. Norris, G. & Brown, S. EPA Positive Matrix Factorization (PMF) 5.0 Fundamentals and User Guide. EPA PMF 5.0 Man, (2014).
50. Polissar, V., Hopke, P. K., Paatero, P., Malm, W. C. & Sisler, J. F. Atmospheric aerosol over Alaska 2. Elemental composition and sources. *J. Geophys. Res.* **103**, 19045–19057 (1998).
51. Belis, C. et al. European guide on air pollution source apportionment with receptor models, EUR 29816 EN (Publications Office of the European Union, Luxembourg, 2019).

## ACKNOWLEDGEMENTS

This project received funding from the European Union's Horizon 2020 research and innovation program (Marie Skłodowska-Curie grant agreement No. 707624). The instruments (ELEMENT XR, Thermo Fisher and LC-Q-TOF/MS- Agilent) employed in this study were supported by the European Regional Development Fund (ERDF;

project No 1166-39417). We also acknowledge support from Swiss Federal funds through the Laboratory of Atmospheric Processes and Their Impacts at EPFL. AN also acknowledges support from the project PyroTRACH (ERC-2016-COG) funded from H2020-EU.1.1.–Excellent Science–European Research Council (ERC), project ID 726165. The authors also acknowledge Prof. N. Mihalopoulos and Prof. M. Kanakidou, who generously provided the use of Univ. of Crete infrastructure for sampling.

## AUTHOR CONTRIBUTIONS

K.V. conceived and designed the study. K.V. and M.T. collected and analyzed data, K.V, S. J. and M.P. contributed data. K.V. C.P, A.N., and R.S. synthesized the data and write the manuscript. All authors commented on the manuscript.

## COMPETING INTERESTS

The authors declare no competing interests.

## ADDITIONAL INFORMATION

**Supplementary information** The online version contains supplementary material available at <https://doi.org/10.1038/s41612-021-00215-5>.

**Correspondence** and requests for materials should be addressed to Kalliopi Violaki.

**Reprints and permission information** is available at <http://www.nature.com/reprints>

**Publisher's note** Springer Nature remains neutral with regard to jurisdictional claims in published maps and institutional affiliations.



**Open Access** This article is licensed under a Creative Commons Attribution 4.0 International License, which permits use, sharing, adaptation, distribution and reproduction in any medium or format, as long as you give appropriate credit to the original author(s) and the source, provide a link to the Creative Commons license, and indicate if changes were made. The images or other third party material in this article are included in the article's Creative Commons license, unless indicated otherwise in a credit line to the material. If material is not included in the article's Creative Commons license and your intended use is not permitted by statutory regulation or exceeds the permitted use, you will need to obtain permission directly from the copyright holder. To view a copy of this license, visit <http://creativecommons.org/licenses/by/4.0/>.

© The Author(s) 2021